

# Interpreting the power spectral density of a fluctuating colloidal current

Stuart F. Knowles,<sup>1</sup> Eleanor K. R. Mackay,<sup>2</sup> and Alice L. Thorneywork<sup>1,2a)</sup>

<sup>1)</sup>*Cavendish Laboratory, Department of Physics, University of Cambridge, JJ Thomson Avenue, Cambridge CB3 0HE, UK*

<sup>2)</sup>*Physical and Theoretical Chemistry Laboratory, South Parks Rd, Oxford, OX1 3QZ UK*

(Dated: 29 April 2024)

The transport of molecules through biological and synthetic nanopores is governed by multiple stochastic processes that lead to noisy, fluctuating currents. Disentangling the characteristics of different noise-generating mechanisms is thus central to better understanding molecular transport at a fundamental level. Here, we study current noise experimentally at the single particle level by imaging colloidal particles driven through microfluidic channels by a difference in fluid pressure. In this scenario, currents fluctuate due to the random arrival times of particles into the channel and the distribution of particle speeds within the channel. We find that this results in a characteristic form of the power spectral density of the current, scaling as  $\sim f^0$ , at low frequencies and  $\sim 1/f^2$  at high frequencies. To rationalise these scalings, we extend a model for shot noise with a finite transit time, borrowed from electronic circuit theory, to include the experimental distribution of transit times and compare this model to the experimental spectra. We find excellent agreement between the data and model across a range of driving pressures within an advection-dominated regime, thereby establishing concrete links between the power spectra scalings and underlying mechanisms for this experimental system. This paves the way for establishing a more systematic understanding of the links between features of power spectra and underlying molecular mechanisms in driven systems.

## I. INTRODUCTION

The ability to sensitively control and manipulate the passage of macromolecules, molecules and ions through nanoscopic pores in a membrane is central to the function of many important emerging technologies, from biomedical sensors<sup>1</sup> to desalination devices<sup>2</sup>. Here, biological membrane proteins represent a gold standard, combining high throughput with exquisite selectivity for specific molecular species<sup>3</sup>. While it is possible to build effective devices around (modified) biological nanopores<sup>4</sup>, recent advances in nanoscale fabrication techniques have motivated efforts to replicate this functionality in synthetic nanopore systems<sup>5</sup>. Such solid state pores could be built to order and would offer key advantages, such as greater robustness and the potential to exploit exotic properties of non-biological materials like graphene<sup>6–9</sup>. Despite significant efforts, the level of control over transport through synthetic pores remains some way off that of their biological analogues<sup>10</sup>, in part due to many open questions surrounding the governing principles of confined transport processes.

One characteristic aspect of transport through nanoscale pores is significant fluctuations in measured currents. Over certain frequency regimes, these fluctuations arise from dynamic processes at the molecular level, such as the thermal fluctuations of ions<sup>11–14</sup> or adsorption to the pore surface<sup>15–17</sup>. As such, interpreting fluctuations in these systems can provide significant information on transport at the molecular level beyond that available from the magnitude of the current alone. In

experiments this is generally approached via interpretation of the power spectral density (PSD) of the current, with ongoing efforts to understand the nature of fluctuations in both biological and synthetic porous systems<sup>18</sup>. In spite of this, *unambiguously* linking measured fluctuations to underlying mechanisms is very challenging even for relatively simple scenarios. This is a consequence of the inherent complexity of molecular systems, particularly when under confinement, which introduces behaviours not seen in bulk. For instance, steric and hydrodynamic interparticle interactions change under confinement, becoming longer ranged and even non-decaying with distance<sup>19–22</sup>. Pore geometry can lead to current rectification<sup>23,24</sup>, with further changes in transport if the confining pore is not rigid but fluctuating<sup>25</sup>. Moreover, interactions of ions and molecules with the confining surface lead to complex electroosmotic flows<sup>26–28</sup>, and adsorption itself has been shown to affect the spectral content of nanopore currents<sup>15,16</sup>.

From an experimental perspective, challenges involved in fabricating nanoscale pores with precisely controlled features also makes interpreting and comparing data from molecular level experiments difficult. In contrast, colloidal models allow for sensitive control of key physicochemical properties, including particle size and shape<sup>29</sup>, interparticle interactions<sup>30,31</sup>, confining geometry<sup>32</sup> and driving force<sup>33,34</sup> in systems where single particle<sup>35,36</sup> and many-body<sup>37</sup> fluctuations can be visualised in detail. This has motivated various experimental studies on microscale transport processes in confinement, examining diffusive behaviour<sup>32,38–40</sup>, the rheological properties of colloidal gels and glasses<sup>41,42</sup>, or driven flows exhibiting clogging and jamming<sup>43–45</sup>. Fluctuations in colloidal transport are, however, comparatively less well explored.

Here, we study fluctuations in the transport of colloidal particles driven through a microfluidic channel to deter-

<sup>a)</sup>alice.thorneywork@chem.ox.ac.uk

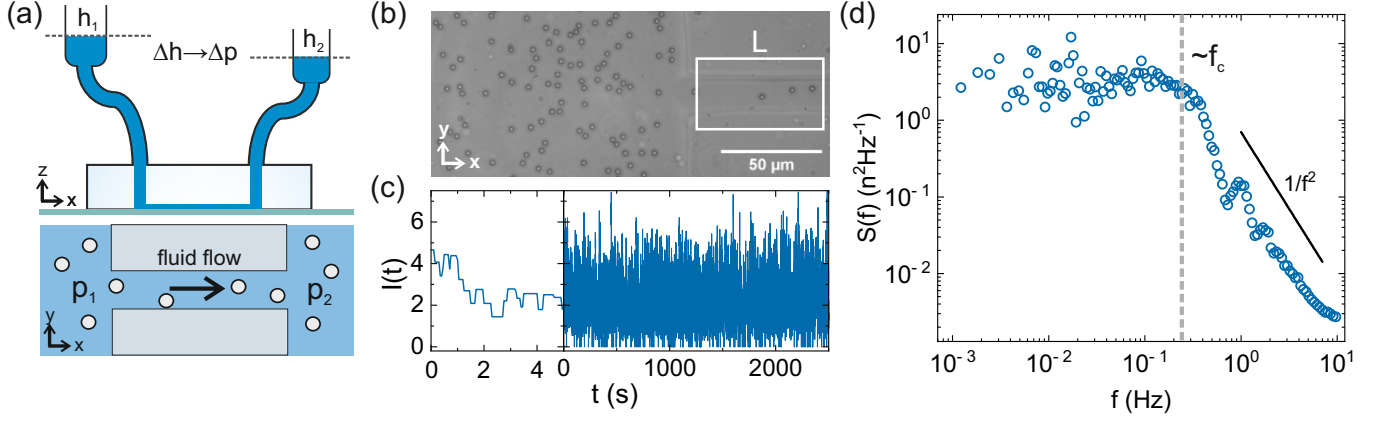


FIG. 1. Quantifying fluctuations in colloidal currents. (a) Schematic of the experimental set-up in which macroscopic reservoirs at different heights produce a pressure difference across the channel. (b) A typical image of the colloidal system (c) The current at two magnifications for a box with  $L = 64 \mu\text{m}$ , showing the arrival/departure of individual particles on short time scales, and the form of the current over longer time scales. (d) The power spectral density calculated from the current in (c).

mine how specific physical mechanisms in this system are manifested in the power spectral density. We first define an approach to calculate currents from individual particle trajectories and subsequently quantify fluctuations in the current via the power spectral density. Our power spectra exhibit a characteristic form, scaling as  $\sim 1/f^2$  at high frequencies and exhibiting white noise,  $\sim f^0$ , at low frequencies. By considering relevant time scales for the particle transport, we link these scaling regimes to key noise-generating mechanisms in this system, namely the random arrival times of particles to the channel and the distribution of particle speeds within it. Finally, by drawing an analogy with noise in electronic circuits, we identify a suitable model for the fluctuations in our system as shot noise with a finite transit time and modify this to include the distribution of particle speeds within the channel. We compare spectra predicted from this model with our measured experimental spectra and find excellent agreement between the two.

## II. EXPERIMENTAL METHODS

The experimental system has previously been reported<sup>46</sup> and is illustrated schematically in Fig. 1(a). This consists of a microfluidic chip designed to include two reservoirs linked by channels with length  $L \sim 100 \mu\text{m}$ , height  $h = 8 \mu\text{m}$  and a width  $14 \mu\text{m}$ . The device is fabricated by replica moulding the main structure in poly-dimethylsiloxane (PDMS) and then plasma bonding this component onto a glass slide coated with a thin layer of PDMS. The chip is filled with a suspension of  $\sigma = 2.8 \mu\text{m}$  carboxylate functionalised melamine formaldehyde particles. The high density of the colloidal particles with respect to the solvent causes them to sediment rapidly onto the base of the chip, forming a quasi-2D monolayer confined by gravity. Following assembly, the microfluidic device is attached to

two macroscopic fluid reservoirs that impose a pressure difference across the chip to drive particles through the channels.

Data was recorded at 20 frames per second for different imposed driving forces using a custom built inverted microscopy set-up. A typical microscopy image of the system is shown in Fig. 1(b). Particle tracking algorithms<sup>47,48</sup> exploiting adaptive linking<sup>46</sup> were used to obtain particle trajectories, with  $\sim 3000$  trajectories contributing to each current. The concentration of particles in the monolayer is defined by a packing fraction,  $\phi = N\pi\sigma^2/4A$ , with  $N$  the number of particles in area  $A$ . Here the system was studied in a low concentration regime with  $\phi \sim 0.07\text{--}0.12$  in the bulk. The colloidal model has previously been shown to be an excellent model hard disk system<sup>49</sup>, and for these low packing fractions and the driving forces used, we do not observe clogging of the channels as seen in other work<sup>43,45</sup>.

## III. RESULTS

### A. Quantifying particle transport as a current

The pressure-driven fluid flow creates an advection dominated transport of particles inside the channels with particles primarily following streamlines parallel to the channel walls<sup>46</sup>. To characterise this transport as a current,

we define a region of interest (ROI) of length  $L$  which spans the width of the channel, as illustrated in Fig. 1(b). When crossing the ROI each particle is defined to contribute a rectangular pulse to the current as:

$$\begin{aligned} i_k(t) &= 1/\tau_k \text{ for } t_0 \leq t \leq t_0 + \tau_k \\ i_k(t) &= 0 \text{ otherwise.} \end{aligned} \quad (1)$$

where  $i_k$  is the current pulse for the  $k$ th particle,  $t_0$  is the time at which the particle enters the channel and  $\tau_k$  is the particle's transit time, i.e. the time for a particle to cross the ROI. The total current can then be found as the sum of all the current pulses:

$$I(t) = \sum_k i_k(t). \quad (2)$$

Fig. 1(c) shows a typical current trace both at fine resolution – where the arrival and departure of individual particles can be seen – and at a longer-time, coarser resolution. By choosing a sufficiently high frame rate we ensure that particle displacements are smaller than  $L$  and that all particles are counted. Eq. 2 results in a mean current that is equal to the mean flux of particles,  $J = cW\bar{v}$ , where  $W$  is the channel width,  $c$  is the particle concentration per unit area in the channel and  $\bar{v}$  is the mean velocity in the channel. Moreover, as division by  $\tau_k$  ensures that the area under each rectangular pulse is 1, the integrated current gives the total number of particles that have passed through the channel up to time  $t$ . We note that the instantaneous value of the current,  $I(t)$ , differs from a measurement of the number of particles crossing some reference line, such as the channel midpoint, per unit time. The two definitions are closely linked, however, in that the case for particles crossing a line reduces to a box with  $L \rightarrow 0$ .

To analyse fluctuations in the current in an analogous way to that employed for nanopore studies, we calculate the power spectral density (PSD) of the current,  $S(f)$ . This can be calculated directly from the Fourier transform of the current,  $I(t)$ , measured over sufficiently long time  $T$ , as:

$$S(f) = \frac{1}{T} |\mathcal{F}\{I(t)\}|^2. \quad (3)$$

To reduce the statistical error on values of  $S(f)$ , we take the average of PSDs calculated from multiple short sections of the total current trace, using Welch's method<sup>50</sup>. The resulting spectra is smoothed further by logarithmically binning along the frequency axis and taking the average noise power in each bin.

A typical PSD for the colloidal current is shown in Fig. 1(d) for  $L = 64 \mu\text{m}$  and a mean particle velocity of  $36.1 \mu\text{ms}^{-1}$ . Despite the simplicity of the model system, the spectra show rich behaviour with two clear regimes: a low frequency regime that exhibits no significant frequency dependence, scaling as  $f^0$ , and a high frequency regime in which the spectra decays approximately as  $1/f^2$  with pronounced oscillations in the decay. The crossover between these two regimes occurs at  $\sim 0.25 \text{ Hz}$ , which corresponds to a time scale on the order of seconds.

For driven transport, the most obvious time scale for the system is the mean time it takes a particle to cross the ROI. For this dataset, this time is  $\sim 2 \text{ s}$ , which is not dissimilar to the crossover frequency. As such, the high frequency regime mainly corresponds to times shorter

than the mean time it takes a particle to cross the ROI, implying that the  $1/f^2$  scaling and oscillations link to the particle transit through the channel. In contrast, the low frequency regime corresponds to behaviour over times longer than the particle transit times, and so instead reflects fluctuations in the current associated with the arrival times of the particles into the channel.

## B. Variation of spectra with ROI length $L$

To further investigate the crossover between the two regimes in the spectra, we next consider the variation in the PSD with the length of the ROI,  $L$ . Fig. 2(a) illustrates the qualitative differences between current traces measured in longer or shorter regions. A larger value of  $L$  corresponds to a more smoothly varying current, comprised of many broad, overlapping pulses, whereas at smaller values of  $L$  the discretisation of current carriers becomes more significant, leading to currents comprised of distinct spikes. While the apparent magnitude of the current increases as  $L$  decreases, this is a consequence of dividing the pulse per particle by the transit time. This ensures that the current as a measure of the mean number of transported particles is independent of the ROI size, despite the fact that the number of particles instantaneously occupying a shorter ROI is lower due to the shorter transit times.

The corresponding spectra are presented in Fig. 2(b). All spectra have the same form as that in Fig. 1(d) with the most notable difference between spectra being the shift in the corner frequency to lower values with increasing  $L$ . This supports the link between corner frequency and mean particle transit time as  $f_c \sim 1/\tau$ , as increasing the length of the ROI will increase the mean transit time.

For low frequencies, the spectra are essentially identical, with a plateau value of approximately double the mean current through the ROI. This is consistent with the picture of a low frequency regime reflecting fluctuations in the arrival of particles into the ROI; the mean current depends on the total number of particles that pass through any region of the channel which is equal to the mean arrival rate due to particle number conservation. The coincidence of the fine structure of the PSD at low frequencies is a consequence of the fact that the current in a larger ROI can be expressed in terms of the current through any smaller ROI within the same channel. This is discussed in Appendix A.

## C. Modelling shot noise with a finite transit time

Having established the phenomenological behaviour of the power spectral density of our system in different frequency regimes we now seek to more quantitatively link features of the PSD to molecular mechanisms. At low frequencies, the dominant mechanism appears to be the small number noise, or 'shot noise', associated with ran-

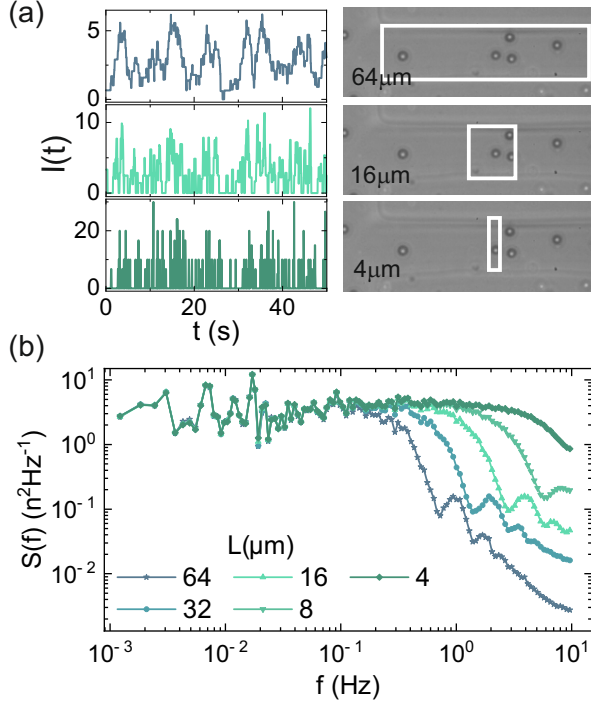


FIG. 2. The dependence of the colloidal current and experimental PSD on ROI size for a mean particle speed within the channel of  $36.1 \mu\text{ms}^{-1}$ . (a) Currents  $I(t)$  for three ROIs of different length,  $L$ , as illustrated in the microscopy images (right). (b) The PSD of the colloidal current fluctuations for five different values of  $L$ .

dom arrival of particles into the channel. This type of noise has been widely studied and extensively characterised in the context of electronic circuits<sup>51,52</sup>. As such, these works provide a starting point for modelling the current in our colloidal system.

If arrival times of current carriers are independent and randomly distributed according to Poisson statistics the power spectral density of a current exhibiting shot noise is independent of frequency, with the form:

$$S_{I,shot}(f) = 2eI_0 \quad (4)$$

for an average current,  $I_0$ , and elementary charge,  $e$ . The root mean squared noise,  $\sigma$ , measured in some finite bandwidth,  $\Delta f$ , is then

$$\sigma = (2eI_0\Delta f)^{1/2}. \quad (5)$$

As the signal to noise ratio for purely shot noise varies with  $I_0^{-1/2}$ , shot noise can be neglected for large currents but is significant for situations where there are small numbers of particles making up the current as in this study.

Pure shot noise assumes that pulses contributing to the current are instantaneous. Yet in many physical systems, pulses have a finite duration, for example due to the time required for a charge carrier to move from emitter to

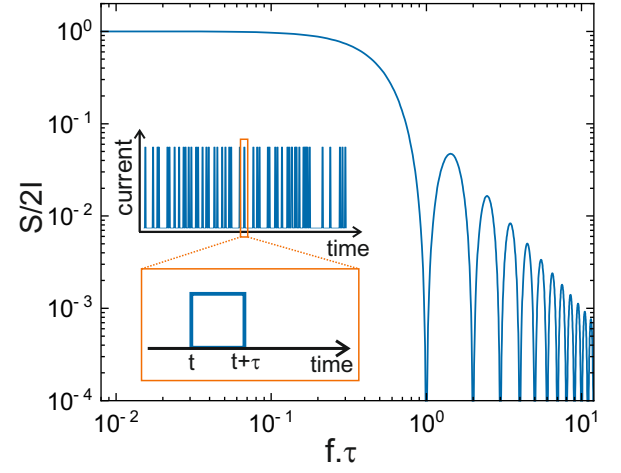


FIG. 3. The PSD of shot noise with a single, finite transit time  $\tau$  as described by Eq. 7. The maximum magnitude of the spectra has been normalised to 1, and the frequency has been rescaled by the characteristic frequency  $1/\tau$ .

detector. This is the scenario for the colloidal model considered here, as pulses have a finite duration equal to the time for particles to cross the ROI (see Eq. (1)). The effect of finite transit times on shot noise can be modelled analytically, and in the following we outline the derivation from MacDonald<sup>51</sup>.

If we assume that all particles cross the channel with the same velocity, every particle will contribute a rectangular pulse of length  $\tau$  to the signal. The real-space autocorrelation function for the current fluctuations can then be expressed in terms of a single pulse,  $i_1(t)$ , starting at  $t = 0$  as:

$$\begin{aligned} \psi(T) &= \langle I(t)I(t+T) \rangle \\ &= I_0 \int_0^\infty i_1(t)i_1(t+T)dt \\ &= I_0 \int_0^{\tau-T} \left(\frac{1}{\tau}\right)^2 dt \\ &= \frac{I_0}{\tau} \left(1 - \frac{T}{\tau}\right). \end{aligned} \quad (6)$$

We can obtain the power spectral density as the Fourier transform of the autocorrelation function as:

$$\begin{aligned} S(f) &= 4 \int_0^\infty \psi(T) \cos(2\pi fT) dT \\ &= \frac{4I_0}{\tau} \int_0^\tau \left(1 - \frac{T}{\tau}\right) \cos(2\pi fT) dT \end{aligned}$$

leading to the final expression:

$$S(f) = \frac{2I_0 \sin^2(\pi f\tau)}{\pi^2 f^2 \tau^2} \quad (7)$$

A plot of Eq. 7 is shown in Fig. 3, where the frequency has been rescaled by the characteristic frequency,  $1/\tau$ , and

the magnitude is rescaled by  $1/2I_0$ . In line with the experimental results the spectra show the same two scaling regimes, separated by a corner frequency,  $f_c = 1/(2\tau)$ . Notably, the PSD also shows characteristic oscillations at high frequencies with zeros at  $f = \frac{n}{\tau}$  for integer values of  $n$ , although these oscillations are much more pronounced than in the experimental spectra in Fig. 1(d).

#### D. Developing a distributed transit time model for the PSD

While the overall form of our experimental current spectra is similar to the transit time model, the two curves do not agree quantitatively using the mean transit time as input. Here, an obvious discrepancy is that the model assumes a single transit time, whereas in the experiment there is a distribution of particle transit times due to the variation of fluid flow speed across the channel width. This suggests that to establish a fully quantitative model, Eq. 7 must be extended to account for the particle transit time distribution.

The first ingredient determining the shape of this distribution is the velocity profile of particles within the channel. This can be calculated directly from the experimental trajectories<sup>46</sup> and a typical example is shown in Fig. 4(a). Particle velocities inside the channel are dominated by advection and so reflect the underlying fluid flow<sup>53</sup>, with corrections for finite particle size and hydrodynamic interactions with the confining walls<sup>54,55</sup>. As such, particle velocities are lowest at the channel walls due to friction and rise towards the channel centre, similar to a Poiseuille flow profile.

The probability distribution for the speed of a randomly selected particle does not exhibit this same functional form, however, as particle streamlines are not uniformly distributed across the channel width. As such, the probability distribution for particle position within the channel,  $P(y)$ , must also be accounted for.  $P(y)$  corresponding to the velocity distribution in (a) is plotted in Fig. 4(b) and shows an excess of particles at the channel walls. This is an excluded volume effect. If a particle enters the channel on a fluid streamline that lies within one particle radius of the channel wall, the particle must be shunted closer to the channel centre, as shown schematically in Fig. 4(c). This creates an enhanced probability of finding particles in a small region close to the walls.

Previous work observed a similar effect, where mean velocities of tracer particles in microchannels were lowered by a bunching of particles at the channel wall<sup>34</sup>. Here, the authors introduced a dimensionless entrance Péclet number, comparing the time to be advected into the channel and the time to diffuse across half its width. Values of  $Pe > \sim 10^3$  are associated with fast capture at the entrance to the channel, meaning particles have insufficient time to redistribute themselves diffusively across channel streamlines. Calculating this quantity in our experiments gives values  $Pe \sim 2 \times 10^3$  and higher, consis-

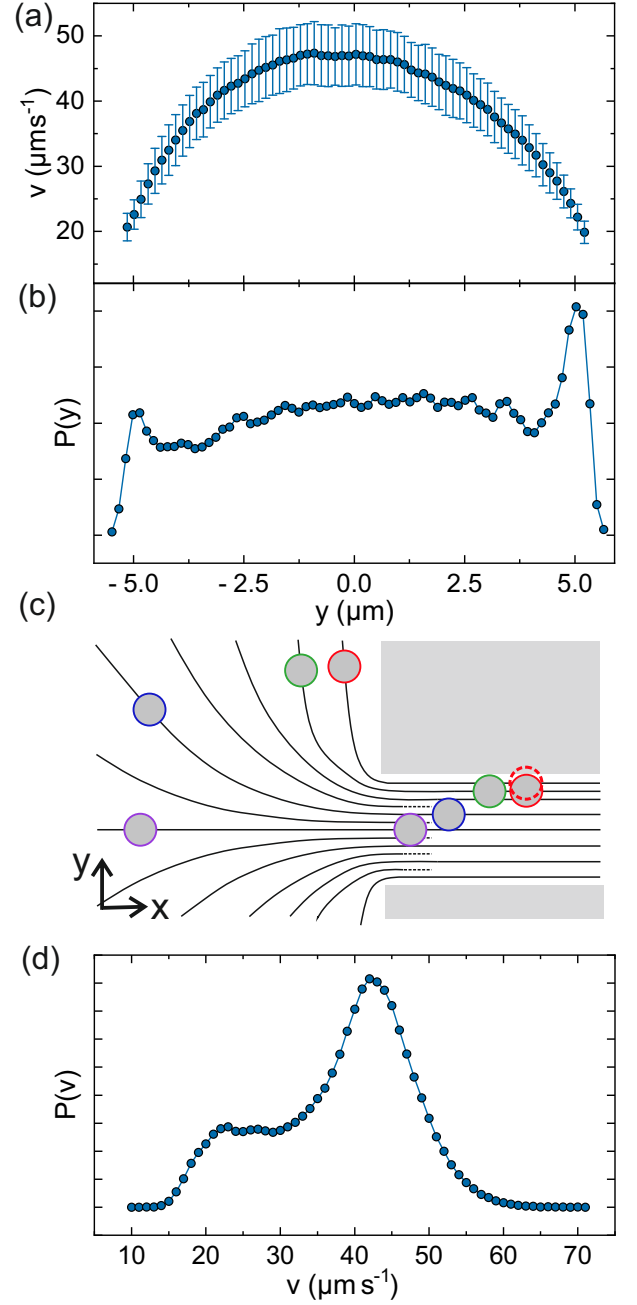


FIG. 4. Distributions of particle position and speed inside the channel. (a) The particle velocity along the channel as a function of distance from the channel centre. Data points show the mean speed with  $\pm$  one standard deviation as error bars. (b) The normalised probability distribution of particle positions across the channel. (c) An illustration of the particle capture process under pressure driven flow at high Peclet number. (d) The distribution of particle speeds within the channel,  $P(v)$ .

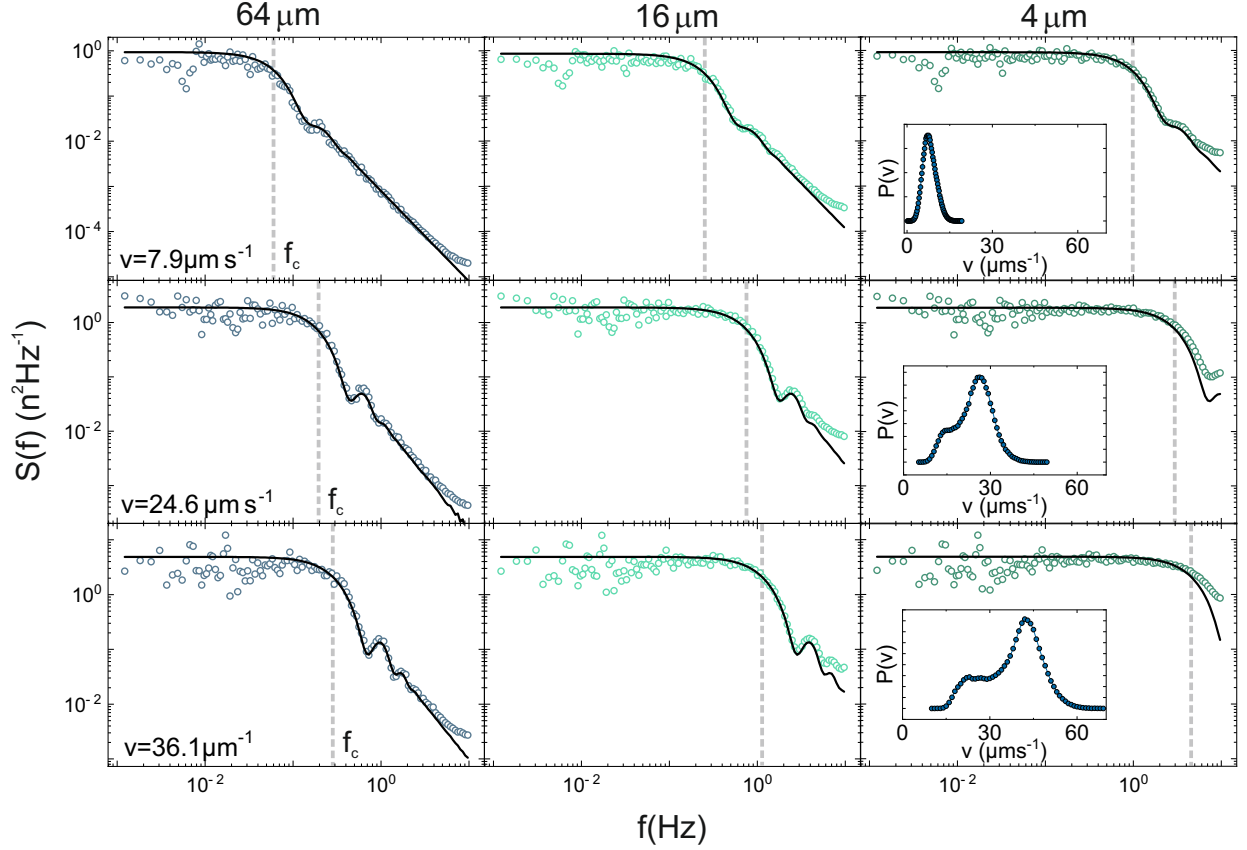


FIG. 5. A comparison between measured (points) and modelled (lines) power spectral densities of colloidal current fluctuations. Rows have constant flow speed, indicated in the leftmost panel, and columns have the same ROI length, indicated at the top of the column. Insets in rightmost panels show the velocity distribution for the three different flow speeds.

tent with this previously predicted regime<sup>34</sup>.

The probability density function for the speed of a randomly chosen particle passing through the channel,  $P(v)$ , follows from  $v(y)$  and  $P(y)$ , and is shown in Fig. 4(d). Here, the probability density  $P(v)$  was obtained directly as a normalised histogram of individual particle velocities within the channel, but can be qualitatively interpreted from the two distributions in panels (a) and (b). In particular, the main peak in  $P(v)$  is at the speed realised in the centre of the channel and the tail at lower velocities comes from the excess of particles at the edge. In the following, we choose the probability distribution of particle velocities  $P(v)$  as the most useful experimental measure of the distribution of particle transit times; compared to a distribution of transit times, it is independent of ROI length and has a finer resolution than measuring channel occupancy times, which are coarsened by the finite frame rate.

To extend Eq. 7, we now proceed by treating the total power spectrum as the sum over power spectra from many independent sources, where each source has a different characteristic transit time arising from the velocity distribution. Firstly, we define  $P(\tau)$  to be the probability density function that a particle crosses the ROI in time

$\tau$ . The contribution to the current comprised of particles transiting in time  $\tau$  is then:

$$I_\tau = I_0 P(\tau) d\tau, \quad (8)$$

where  $I$  is the total average current. From Eq. 7 we obtain a differential spectrum,  $dS$ :

$$dS(f, \tau) = 2I_0 P(\tau) \frac{\sin^2(\pi f \tau)}{\pi^2 f^2 \tau^2} d\tau, \quad (9)$$

which can be integrated to obtain the full spectrum:

$$S_{\text{model}}(f) = \frac{2I_0}{\pi^2 f^2} \int_0^\infty \frac{P(\tau) \sin^2(\pi f \tau)}{\tau^2} d\tau. \quad (10)$$

This is a complete model for the PSD of shot noise fluctuations in a current with a distribution of transit times. If we transform this into the particle speed domain, which is experimentally more convenient, we have  $\tau = L/v$  and  $P(\tau) d\tau = P(v) dv$

$$S_{\text{model}}(f) = \frac{2I_0}{\pi^2 L^2 f^2} \int_0^\infty P(v) v^2 \sin^2 \frac{\pi f L}{v} dv. \quad (11)$$

The low frequency limit of Eq. 11 is:

$$\lim_{f \rightarrow 0} S_{\text{model}} = 2I_0,$$

showing that at long times the spectral density of pure shot noise is recovered.

The distributed transit time model retains many features of the single transit time model. Firstly, there is a corner frequency  $f_c = 1/(2\tau)$ , now at a characteristic average transit time, separating  $f^0$  and  $f^{-2}$  noise regimes. The  $f^0$  scaling arises due to the independent random arrival of particles, while the  $f^{-2}$  scaling arises from the linear scaling in the autocorrelation function, a consequence of the uniform velocity of particles as they transit across the ROI. The key difference is that oscillations are smoothed out in the distributed transit time model. This smoothing is sensitive to the distribution of particle transit times. For example, a wider distribution of transit times (or a narrower distribution of particle speeds) creates more smoothing out of these oscillations.

Finally, in Fig. 5 we show a comparison between the model spectrum of Eq. 11 (solid line) and the experimental data (points) for three different flow speeds and three different values of  $L$ . In all cases, the modelled spectrum was evaluated from Eq. 11 as a sum over the experimental distributions for  $P(v)$  (shown as insets) with the mean current  $I_0$  calculated directly from the measured particle currents. Excellent agreement is seen in all cases across four decades of frequency, especially in the size and location of the oscillations at around 1 Hz for larger ROIs. The corner frequencies are also a good match to  $f_c = 1/(2\tau) = \bar{v}/(2L)$ , using the mean particle speed as input. At low frequencies, the theoretical expression appears to slightly overestimate the height of the plateau, and the data rises above the model slightly at the highest frequencies due to aliasing of the spectrum<sup>56</sup>. We emphasise, however, that in comparing Eq. 11 to the experimental data here, there are no free fitting parameters: the only inputs are the defined ROI length,  $L$ , along with the average current,  $I_0$ , and the speed distribution,  $P(v)$  which are measured directly from the particle trajectories.

#### IV. DISCUSSION AND CONCLUSIONS

In this paper, we have explored the fluctuation behaviour of low-density currents of colloidal particles driven through confining channels in a microfluidic device. Inspired by experiments on nanopore transport, we quantify fluctuations by calculation of the power spectral density (PSD) of the current with the goal to link features of the PSD to underlying physical mechanism. Despite the relative simplicity of the experiment, the power spectral density of the current fluctuations through the channel shows rich behaviour, with multiple characteristic features. For this well-defined and observable experimental system, however, we can unambiguously link these features to specific aspects of the colloidal dynamics as follows.

- The PSD shows two characteristic scaling regimes separated by a corner frequency,  $f_c$ , which re-

flects the time it takes a particle to cross the ROI. As such, the high frequency scaling regime relates to times that are short compared to this transit time and reflects transport of the particle through the channel itself. In contrast, the low frequency regime relates to a fluctuation mechanism operating over much longer time scales. An obvious candidate for the low frequency behaviour is fluctuations in the entrance of particles into the channel.

- At low frequencies, we find a scaling as  $f^0$ , implying that arrival times of particles into the channel are uncorrelated. We have previously shown that particle transport into the channel depends upon the time for drift-diffusion across the reservoir to a capture region<sup>46</sup>. For the semi-dilute packing fractions studied here, the mean distance between particles is relatively large and so interparticle interactions do not significantly influence dynamics. As such, particles do not impede each other and enter the channel independently, consistent with our observation of low frequency white noise.
- The amplitude of the low frequency regime is approximately twice the average current through the ROI. This is the low frequency limit predicted for shot noise.
- At high frequencies, we see a decay as  $1/f^2$  as the finite time for particles to pass through the channel leads to time-dependent correlations in the particle current. Observation of a scaling of  $1/f^2$  reflects the directed, advective transport of particles. This is distinct from diffusive transport through channels<sup>11</sup>, which been observed to lead to an alternative scaling of  $1/f^{3/2}$ .
- The high frequency regime exhibits characteristic oscillations that arise from the finite transit time of particles through the channel. The extent to which these are observed depends on the distribution of transit times, a consequence of the distribution of particle velocities within the channel. Inside our microfluidic devices, the distribution of transit times has a complex functional form that can be rationalised by consideration of the nonuniform velocity profile across the channel width and nonuniform distribution of particle positions. In general, however, oscillations in the PSD are more or less pronounced depending on the width of the distribution, with a narrower range of transit times giving larger amplitude oscillations.

This combination of PSD features is reminiscent of models for shot noise with a finite transit time developed for electronic noise. Despite the obvious physical differences between the two systems, we have shown that by modifying such expressions to allow for a distribution of finite transit times we can quantitatively model the experimental power spectral density of our colloidal



currents. This highlights firstly how widespread these particular noise creating mechanisms are across physical systems and secondly the potential for translating models from the well-studied area of electronic noise to understand fluctuations in soft systems. Moreover, comparison to these shot noise models demonstrates that while the characteristic scalings of the PSD can be explained by rather general mechanisms, more specific details of the system, for example, the velocity distribution arising from our specific microfluidic geometry, are required to achieve a full quantitative understanding.

Our experimental model is heavily simplified in comparison to synthetic and biological nanoscale pores, but its key features are still relevant. Molecular currents are also comprised of randomly arriving current-carrying particles and as such similar signatures in the PSD could in principle be observed for molecular transport. Moreover, while the range of transit times in the colloidal model was due to the particle velocity distributions as we worked in an advection-dominated regime, distributions of transit times due to stochastic variation in diffusive transport could be explored in a similar manner.

More broadly, having fully and unambiguously established the behaviour of the power spectra for the simple case of a non-interacting current of hard spheres, this experimental platform offers an opportunity to investigate the impact of more complex phenomena on the PSD. For example, in highly crowded molecular systems capture of particles may no longer be independent, which would require an extension of the analytical model to account for interactions. Moreover, many open questions remain about the origin of low frequency  $f^{-1}$  scaling of the fluctuations in nanopores. Recent work has suggested that this scaling arises as a consequence of particle dynamics in the reservoir rather than in the channels themselves<sup>17,57</sup> and resolving such behaviour in our colloidal model will be the object of future work.

## DATA AVAILABILITY

All data needed to evaluate the conclusions in the paper are present in the paper. Other data are available upon reasonable request to the corresponding author.

## ACKNOWLEDGMENTS

We wish to acknowledge useful discussions with Roel Dullens, Ulrich Keyser and Sophie Marbach. S. F. K. acknowledges funding from UK Research and Innovation -Engineering and Physical Sciences Research Council (UKRI, EPSRC) and the EPSRC CDT in Nanoscience and Nanotechnology (NanoDTC). A.L.T. acknowledges funding from a Royal Society University Research Fellowship (URF\R1\211033). E.K.R.M. and A.L.T. acknowledge funding from EPSRC (EP/X02492X/1).

## APPENDIX A: COINCIDENCE OF LOW-FREQUENCY FINE STRUCTURE IN THE PSD

Consider an ROI of length  $L$  that can be divided into  $n$  subsections of length  $L/n$ . Here, the current through the large ROI can be directly related to that through the smaller ROIs as:

$$I_L(t) = \frac{1}{n} \sum_{j=0}^{n-1} I_{L/n,j}(t) \quad (12)$$

where  $I_L(t)$  refers to the current through an ROI of length  $L$  and  $I_{L/n,j}(t)$  the current through the  $j^{\text{th}}$  ROI of length  $L/n$ . Within the channel, the particle dynamics are dominated by advection. As such, to first order, the currents through adjacent sub-ROIs are the same except for an offset in time,  $\tau$ , equal to the mean particle transit time through the sub-ROI,

$$I_{L/n,j}(t) \approx I_{L/n,j-1}(t - \tau). \quad (13)$$

allowing Eq. 12 to be expressed as

$$I_L(t) \approx \frac{1}{n} \sum_{j=0}^{n-1} I_{L/n,0}(t - j\tau). \quad (14)$$

The power spectrum of the current through the large ROI,  $S_I$ , is then

$$\begin{aligned} S_I &= |\mathcal{F}\{I_L(t)\}|^2 \\ &\approx \left| \mathcal{F} \left\{ \frac{1}{n} \sum_{j=0}^{n-1} I_{L/n,0}(t - j\tau) \right\} \right|^2 \\ &= \frac{1}{n^2} \left| \sum_{j=0}^{n-1} \tilde{I}_{L/n,0}(f) e^{-2\pi i j \tau f} \right|^2 \\ &= \frac{1}{n^2} \left| \tilde{I}_{L/n,0}(f) \right|^2 \left| \sum_{j=0}^{n-1} e^{-2\pi i j \tau f} \right|^2. \end{aligned} \quad (15)$$

where in step two we use the identity for Fourier transforms with a time shift,

$$\mathcal{F}\{x(t - \tau)\} = \mathcal{F}\{x(t)\} e^{2\pi i \tau f} = \tilde{x}(f) e^{2\pi i \tau f}$$

with  $\tilde{x}$  the Fourier transform of  $x$ . At low frequencies, where

$$2\pi \tau f \ll 1 \quad (16)$$

all of the terms in the final sum of Eq. 15 are approximately equal to 1. In this regime,

$$\begin{aligned} S_I &= \frac{1}{n^2} \left| \tilde{I}_{L/n,0}(f) \right|^2 \times n^2 \\ |\mathcal{F}\{I_L(t)\}|^2 &= |\mathcal{F}\{I_{L/n,0}(t)\}|^2 \end{aligned} \quad (17)$$

That is, at sufficiently low frequencies the PSD for the fluctuations in the current through a small ROI equals that through a large ROI.



- <sup>1</sup>S. Howorka and Z. Siwy, “Nanopore analytics: Sensing of single molecules,” *Chemical Society Reviews* **38**, 2360–2384 (2009).
- <sup>2</sup>J. R. Werber, C. O. Osuji, and M. Elimelech, “Materials for next-generation desalination and water purification membranes,” *Nature Reviews Materials* **1** (2016), 10.1038/natrevmats.2016.18.
- <sup>3</sup>H. B. Park, J. Kamcev, L. M. Robeson, M. Elimelech, and B. D. Freeman, “Maximizing the right stuff: The trade-off between membrane permeability and selectivity,” *Science* **356**, eaab0530 (2017).
- <sup>4</sup>J. Schmidt, “Membrane platforms for biological nanopore sensing and sequencing,” *Current Opinion in Biotechnology* **39**, 17–27 (2016).
- <sup>5</sup>C. Dekker, “Solid-state nanopores,” *Nature Nanotechnology* **2**, 209–215 (2007).
- <sup>6</sup>S. Sahu and M. Zwolak, “Colloquium: Ionic phenomena in nanoscale pores through 2d materials,” *Rev. Mod. Phys.* **91**, 021004 (2019).
- <sup>7</sup>B. Radha, A. Esfandiari, F. Wang, A. Rooney, K. Gopinadhan, A. Keerthi, A. Mishchenko, A. Janardanan, P. Blake, L. Fumagalli, M. Lozada-Hidalgo, S. Garaj, S. J. Haigh, I. V. Grigorieva, H. A. Wu, and A. K. Geim, “Molecular transport through capillaries made with atomic-scale precision,” *Nature* **538**, 222–225 (2016).
- <sup>8</sup>T. Emmerich, K. S. Vasu, A. Niguès, A. Keerthi, B. Radha, A. Siria, and L. Bocquet, “Enhanced nanofluidic transport in activated carbon nanoconduits,” *Nature Materials* **21** (2022), 10.1038/s41563-022-01229-x.
- <sup>9</sup>M. Caglar, I. Silkina, B. T. Brown, A. L. Thorneywork, O. J. Burton, V. Babenko, S. M. Gilbert, A. Zettl, S. Hofmann, and U. F. Keyser, “Tunable anion-selective transport through monolayer graphene and hexagonal boron nitride,” *ACS Nano* **14**, 2729–2738 (2020).
- <sup>10</sup>P. Robin and L. Bocquet, “Nanofluidics at the crossroads,” *Journal of Chemical Physics* **158** (2023), 10.1063/5.0143222.
- <sup>11</sup>S. Marbach, “Intrinsic fractional noise in nanopores: The effect of reservoirs,” *The Journal of Chemical Physics* **154** (2021), 10.1063/5.0047380.
- <sup>12</sup>S. F. Knowles, U. F. Keyser, and A. L. Thorneywork, “Noise properties of rectifying and non-rectifying nanopores,” *Nanotechnology* **31**, 10LT01 (2020).
- <sup>13</sup>R. M. M. Smeets, U. F. Keyser, N. H. Dekker, and C. Dekker, “Noise in solid-state nanopores,” *Proc. Natl. Acad. Sci. U.S.A.* **105**, 417–421 (2008).
- <sup>14</sup>S. M. Bezrukov, A. M. Berezhkovskii, M. A. Pustovoi, and A. Szabo, “Particle number fluctuations in a membrane channel,” *The Journal of Chemical Physics* **113**, 8206–8211 (2000).
- <sup>15</sup>S. F. Knowles, N. E. Weckman, V. J. Lim, D. J. Bonthuis, U. F. Keyser, and A. L. Thorneywork, “Current fluctuations in nanopores reveal the polymer-wall adsorption potential,” *Physical Review Letters* **127** (2021), 10.1103/PhysRevLett.127.137801.
- <sup>16</sup>S. Gravelle, R. R. Netz, and L. Bocquet, “Adsorption kinetics in open nanopores as a source of low-frequency noise,” *Nano Letters* **19**, 7265–7272 (2019).
- <sup>17</sup>P. Robin, M. Lizée, Q. Yang, T. Emmerich, A. Siria, and L. Bocquet, “Disentangling 1/f noise from confined ion dynamics,” *Faraday Discussions* (2023), 10.1039/d3fd00035d.
- <sup>18</sup>A. Fragasso, S. Schmid, and C. Dekker, “Comparing current noise in biological and solid-state nanopores,” *ACS Nano* **14**, 1338–1349 (2020).
- <sup>19</sup>B. Cui, H. Diamant, B. Lin, and S. A. Rice, “Anomalous hydrodynamic interaction in a quasi-two-dimensional suspension,” *Phys. Rev. Lett.* **92**, 258301 (2004).
- <sup>20</sup>K. Misiunas, S. Pagliara, E. Lauga, J. R. Lister, and U. F. Keyser, “Nondecaying hydrodynamic interactions along narrow channels,” *Phys. Rev. Lett.* **115**, 038301 (2015).
- <sup>21</sup>Q. H. Wei, C. Bechinger, and P. Leiderer, “Single-file diffusion of colloids in one-dimensional channels,” *Science* **287**, 625–628 (2000).
- <sup>22</sup>P. Robin, A. Delahais, L. Bocquet, and N. Kavokine, “Ion filling of a one-dimensional nanofluidic channel in the interaction confinement regime,” *The Journal of Chemical Physics* **158**, 124703 (2023).
- <sup>23</sup>M. R. Powell, N. Sa, M. Davenport, K. Healy, I. Vlassiuk, S. E. Létant, L. A. Baker, and Z. S. Siwy, “Noise properties of rectifying nanopores,” *J. Phys. Chem. C* **115**, 8775–8783 (2011).
- <sup>24</sup>M. Aarts, W. Q. Boon, B. Cuénod, M. Dijkstra, R. V. Roij, and E. Alarcon-Llado, “Ion current rectification and long-range interference in conical silicon micropores,” *ACS Applied Materials and Interfaces* **14**, 56226–56236 (2022).
- <sup>25</sup>S. Marbach, D. S. Dean, and L. Bocquet, “Transport and dispersion across wiggling nanopores,” *Nature Physics* **14** (2018), 10.1038/s41567-018-0239-0.
- <sup>26</sup>M. Firnkes, D. Pedone, J. Knezevic, M. Döblinger, and U. Rant, “Electrically facilitated translocations of proteins through silicon nitride nanopores: Conjoint and competitive action of diffusion, electrophoresis, and electroosmosis,” *Nano Letters* **10**, 2162–2167 (2010).
- <sup>27</sup>J. Mc Hugh, K. Andresen, and U. F. Keyser, “Cation dependent electroosmotic flow in glass nanopores,” *Applied Physics Letters* **115**, 113702 (2019).
- <sup>28</sup>A. Gubbiotti, M. Baldelli, G. D. Muccio, P. Magaretti, S. Marbach, and M. Chinappi, “Electroosmosis in nanopores: computational methods and technological applications,” (2022).
- <sup>29</sup>S. Sacanna, M. Korpics, K. Rodriguez, L. Colón-Meléndez, S.-H. Kim, D. J. Pine, and G.-R. Yi, “Shaping colloids for self-assembly,” *Nature communications* **4**, 1688 (2013).
- <sup>30</sup>A. Yethiraj and A. V. Blaaderen, “A colloidal model system with an interaction tunable from hard sphere to soft and dipolar,” *Nature* **413**, 513 (2003).
- <sup>31</sup>C. Royall, M. E. Leunissen, and A. van Blaaderen, “A new colloidal model system to study long-range interactions quantitatively in real space,” *Journal of Physics: ...* **15**, S3581 (2003).
- <sup>32</sup>X. Yang, C. Liu, Y. Li, F. Marchesoni, P. Hänggi, and H. P. Zhang, “Hydrodynamic and entropic effects on colloidal diffusion in corrugated channels,” *Proc. Natl. Acad. Sci. U.S.A.* **114**, 9564 (2017).
- <sup>33</sup>K. Misiunas and U. F. Keyser, “Density-dependent speed-up of particle transport in channels,” *Physical Review Letters* **122** (2019), 10.1103/PhysRevLett.122.214501.
- <sup>34</sup>O. Liot, M. Socol, L. Garcia, J. Thiéry, A. Figarol, A. F. Mingotaud, and P. Joseph, “Transport of nano-objects in narrow channels: Influence of brownian diffusion, confinement and particle nature,” *Journal of Physics Condensed Matter* **30** (2018), 10.1088/1361-648X/aac0af.
- <sup>35</sup>T. Franosch, M. Grimm, M. Belushkin, F. M. Mor, G. Foffi, L. Forró, and S. Jeney, “Resonances arising from hydrodynamic memory in brownian motion,” *Nature* **478** (2011), 10.1038/nature10498.
- <sup>36</sup>D. Krapf, N. Lukat, E. Marinari, R. Metzler, G. Oshanin, C. Selhuber-Unkel, A. Squarcini, L. Stadler, M. Weiss, and X. Xu, “Spectral content of a single non-brownian trajectory,” *Physical Review X* **9** (2019), 10.1103/PhysRevX.9.011019.
- <sup>37</sup>E. K. R. Mackay, B. Sprinkle, S. Marbach, and A. L. Thorneywork, (2023), arXiv preprint arXiv:2311.00647.
- <sup>38</sup>U. Siems, C. Kreuter, A. Erbe, N. Schwierz, S. Sengupta, P. Leiderer, and P. Nielaba, “Non-monotonic crossover from single-file to regular diffusion in micro-channels,” *Scientific Reports* **2**, 2–5 (2012).
- <sup>39</sup>S. L. Dettmer, S. Pagliara, K. Misiunas, and U. F. Keyser, “Anisotropic diffusion of spherical particles in closely confining microchannels,” *Phys. Rev. E* **89**, 062305 (2014).
- <sup>40</sup>A. L. Thorneywork, J. Gladrow, Y. Qing, M. Rico-Pasto, F. Rittort, H. Bayley, A. B. Kolomeisky, and U. F. Keyser, “Direct detection of molecular intermediates from first-passage times,” *Science Advances* **6**, 1–7 (2020).
- <sup>41</sup>L. Isa, R. Besseling, and W. C. K. Poon, “Shear zones and wall slip in the capillary flow of concentrated colloidal suspensions,” *Phys. Rev. Lett.* **98**, 198305 (2007).

- <sup>42</sup>J. C. Conrad and J. A. Lewis, “Structure of colloidal gels during microchannel flow,” *Langmuir* **24**, 7628–7634 (2008).
- <sup>43</sup>H. M. Wyss, D. L. Blair, J. F. Morris, H. A. Stone, and D. A. Weitz, “Mechanism for clogging of microchannels,” *Physical Review E - Statistical, Nonlinear, and Soft Matter Physics* **74**, 1–4 (2006).
- <sup>44</sup>A. Marin, H. Lhuissier, M. Rossi, and C. J. Kähler, “Clogging in constricted suspension flows,” *Physical Review E* **97**, 1–5 (2018).
- <sup>45</sup>M. Souzy, I. Zuriguel, and A. Marin, “Transition from clogging to continuous flow in constricted particle suspensions,” *Physical review. E* **101**, 060901 (2020).
- <sup>46</sup>S. F. Knowles, M. Fletcher, J. M. Hugh, M. Earle, U. F. Keyser, and A. L. Thorneywork, “Observing capture with a colloidal model membrane channel,” *Journal of Physics Condensed Matter* **34** (2022), 10.1088/1361-648X/ac7764.
- <sup>47</sup>J. C. Crocker and D. G. Grier, “Methods of digital video microscopy for colloidal studies,” *Journal of colloid and interface science* **179**, 298–310 (1996).
- <sup>48</sup>D. B. Allan, T. Caswell, N. C. Keim, C. M. van der Wel, and R. W. Verweij, “soft-matter/trackpy: v0.6.1,” (2023).
- <sup>49</sup>A. L. Thorneywork, R. Roth, D. G. A. L. Aarts, and R. P. A. Dullens, “Communication: Radial distribution functions in a two-dimensional binary colloidal hard sphere system,” *Journal of Chemical Physics* **140** (2014), 10.1063/1.4872365.
- <sup>50</sup>W. H. Press, S. A. Teukolsky, W. T. Vetterling, and B. P. Flannery, *Numerical Recipes in C: The Art of Scientific Computing* (Cambridge University Press, 1992).
- <sup>51</sup>D. K. C. MacDonald, *Noise and Fluctuations: An Introduction* (Dover Publications, 2006).
- <sup>52</sup>S. Kogan, *Electronic Noise and Fluctuations in Solids* (Cambridge University Press, 1996).
- <sup>53</sup>E. Guazzelli and J. F. Morris, *A physical introduction to suspension dynamics*, Vol. 45 (Cambridge University Press, 2011).
- <sup>54</sup>S. B. Chen and X. Ye, “Faxen’s laws of a composite sphere under creeping flow conditions,” *Journal of Colloid and Interface Science* **221**, 50–57 (2000).
- <sup>55</sup>L. Pasol, M. Martin, M. Ekiel-Jezewska, E. Wajnryb, J. BŁawdziewicz, and F. Feuillebois, “Motion of a sphere parallel to plane walls in a poiseuille flow. application to field-flow fractionation and hydrodynamic chromatography,” *Chemical Engineering Science* **66**, 4078–4089 (2011).
- <sup>56</sup>J. W. Kirchner, “Aliasing in  $1/f^\alpha$  noise spectra: Origins, consequences, and remedies,” *Phys. Rev. E* **71**, 066110 (2005).
- <sup>57</sup>A. Fragasso, S. Pud, and C. Dekker, “ $1/f$  noise in solid-state nanopores is governed by access and surface regions,” *Nanotechnology* **30**, 395202 (2019).